Hindawi
Mathematical Problems in Engineering
Volume 2022, Article ID 7445434, 9 pages
https://doi.org/10.1155/2022/7445434

Research Article

Vibration and Constitutive Relations of Viscoelastic Cantilever Beam of HTPB Propellant

Bo Gao and Zhuo Li

College of Science, Inner Mongolia University of Technology, Hohhot 010051, China

Correspondence should be addressed to Bo Gao; 20181000007@imut.edu.cn

Received 29 March 2022; Revised 20 April 2022; Accepted 26 April 2022; Published 1 June 2022

Academic Editor: Zhihan Lv

A cantilever beam test specimen of a viscoelastic material, which is sourced from the hydroxy-terminated polybutadiene (HTPB) propellant, has been made. The traditional experimental modal analysis (EMA) is performed using the SIEMENS TESTLAB software to obtain the first six orders of modal frequencies based on the Poly MAX method, thereby determining the frequency range associated with the frequency domain analysis. The relaxation modulus of this viscoelastic material is first measured using a thermo-viscoelasticity analyzer (DMA); subsequently, the relaxation modulus is adopted to fit the 19-parameter Prony series of conformational models that characterize this viscoelastic material. Sinusoidal frequency sweep is then conducted on the SIEMENS TESTLAB platform, and the corresponding measured signals are obtained. Using the finite element method, a transient analysis simulation of the experimental conditions is performed. The dynamic response of this viscoelastic material under sinusoidal frequency sweep is evaluated by comparing it with the experimental data. It is observed that the overall acceleration peak error and the finite element simulation result are less than 3%. This study verifies that the obtained static constitutive equation (19-parameter Prony series) can describe the dynamic responses at low frequencies (<80 Hz).

1. Introduction

The propellant grain of a solid rocket motor is regarded as a typical viscoelastic material. When viscoelastic materials are subjected to simple loading conditions, the subsequent deformation process changes with time and the recovery process after unloading is delayed. Therefore, the stress in such a material is not only related to the strain at that time but also to the entire change history of strain. During the recovery process, the one-to-one correspondence between stress and strain no longer exists, and the material undergoes creep and relaxation. Therefore, elucidating the creep or relaxation function of a viscoelastic material has become an important tool to describe its model parameters [1], which is also software friendly. Hui et al. studied the fitting of the shear relaxation modulus function of viscoelastic materials, while exploring the relaxation modulus of a viscoelastic prototype based on Maxwell model [2]. Xu et al. put forward a data fitting method according to a Prony series based on the static tension relaxation experiment and linear viscoelasticity; subsequently, they implemented isokinetic stretching and the relaxation experiment to assess their method [3]. This method also works very well in finite elements. Miller et al. used the conventional method of testing the propellant under uniaxial tension, and the double cantilever beam mode was used to test the propellant in a thermo-viscoelasticity analyzer (DMA); they proved that when the results of the two methods were similar, DMA required less materials, exhibited lower variability, and showed insensitivity to the applied strain [4, 5]. He used the finite element method to simulate and analyze the two-dimensional axial deformation of viscoelastic components, the influence of the viscoelasticity of the material on the model, and viscoelastic behaviors under cyclic loading [6, 7]. A finite element model of asphalt pavements consisting of the Burgers model is presented, where the HTPB propellant was modeled as a viscoelastic material in finite element simulations [8]. Wang adopted the finite element method to study

the viscoelastic responses of buried pipe-type conductive asphalt pavements under moving loads; they implemented a method to convert the constitutive model of viscoelasticity of asphalt mixtures into a Prony series [9, 10]. Zhao et al. calculated the unit response equations associated with three kinds of responses of typical asphalt pavement structures; subsequently, they analyzed the viscoelastic responses of the pavement structure under a semisinusoidal pulse load by using Boltzmann superposition principle [11]. The influence of driving speed on three kinds of viscoelastic responses was also determined. The study indicated that the unit response equation could be accurately expressed by a Prony series, and its parameters could be determined using a configuration method. Wang and Zhang derived the viscoelastic integral-type incremental constitutive equation and its recursive formula (expressed by Kirchhoff stress and Green strain) using a Prony series, thereby proposing a finite element incremental superposition method for calculating the dynamic response to a 3D viscoelastic deformation [12]. Yuan and Sun derived the viscoelasticity constitutive equation of resin (expressed by a Prony series) and set the component material parameters of the model [13]. Shi et al. established the viscoelasticity constitutive model of a Kelvin-like body, which was compared with the classical Prony series model [14, 15].

In service, hydroxy-terminated polybutadiene (HTPB) is subjected to dynamic loading caused by flight and transportation vibrations as well as other environments [16]. It is quite important to determine the short-term and long-term adverse effects of these vibrations on the propellant. Baqersad et al. analyzed the characteristics of vibration response under random excitation [17]. The neural network was adopted to predict the displacement response, and the interval modeling technique was used to construct the damage index. The damage time was determined, and the cantilever beam model was simulated [18]. Zhu and Deng conducted the dynamic response analysis of the cantilever beam with cracks by using the finite element method, and the life of the structure was analyzed [19]. In addition, many scholars have also done a lot of research on solid pellets of HTPB [20–23].

The previous research only studied mechanical properties under static or dynamic conditions, and there were relatively few research studies on the combination of static and dynamic. In the past, the dynamic model of HTPB propellant was very dependent on frequency (including high and low frequencies), so it was difficult to obtain an accurate dynamic model. The fundamental frequency of a solid rocket motor plays a very important role in all vibration frequencies. The fundamental frequency of a solid rocket motor is generally around 80 Hz, so it is very meaningful to study the vibration at low frequencies. This study focuses on the application of the static model of HTPB propellant to the dynamic response at low frequencies, combined with the accuracy of the dynamic model, and avoids the cumbersome acquisition of the dynamic model. The study starts from the basic theory of viscoelasticity and expresses the relaxation modulus as a Prony series to determine the constitutive equation of this viscoelastic material. Then, a sine sweep frequency excitation was conducted to verify that this constitutive equation can be applied in the low-frequency dynamic response.

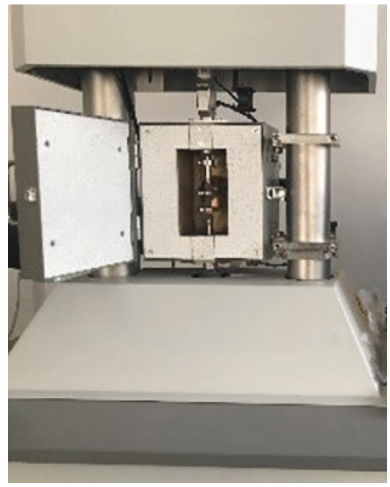

Figure 1: Advanced dynamic thermomechanical analyzer (DMA).

2. Constitutive Equation

2.1. Equipment for the Relaxation Experiment. An advanced dynamic thermomechanical analyzer (EPLEXOR8) developed by German GABO has been used in this study, as shown in Figure 1. The instrument is equipped with two upper and lower driving systems, and the static and dynamic forces are provided by two independent systems. The instrument exhibits a good driving control ability and accuracy, while the test data demonstrate satisfactory repeatability.

2.2. Sample Preparation and Experimental Method. The viscoelastic material is sourced from the HTPB propellant (butyl propellant), which is composed of 68% ammonium perchlorate (AP), 11.3% hydroxy-terminated butadiene (HTPB), 17% aluminum powder (Al), and small amounts of curing agent, plasticizer, and process additive; AP, HTPB, and Al function as an oxidizer, an adhesive, and a metal combustion agent, respectively. The HTPB propellant is one of the commonly used solid propellants in rocket weapons.

This paper obtained the HTPB propellant from China Aerospace Science and Industry Group Sixth Research Institute, as shown in Figure 2. More than eighteen specimens with dimensions of 1.5 mm × 3.5 mm × 7.5 mm are obtained using a special cutter. Three specimens for each temperature. According to the Aerospace Industry Standard of the Ministry of Aeronautics and Astronautics of the People's Republic of China QJ2487-93 [24], the tensile experiments at rate of 500 mm/min and the relaxation modulus are calculated using a DMA since the DMA calculated the relaxation modulus using the measured data, as shown in equation (1). Accordingly, the constitutive model of viscoelasticity, which is characterized by the relaxation modulus, has been established. This study adopts the constitutive equation acquisition method according to the Aerospace

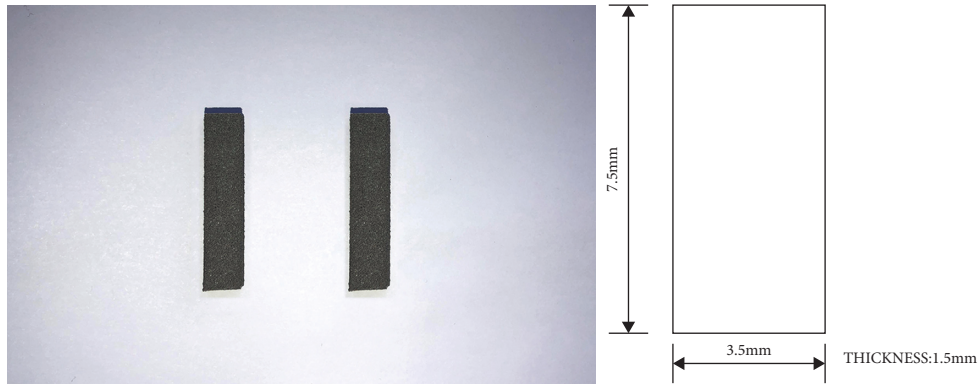

Figure 2: Experiment specimens.

Table 1: Relaxation modulus test conditions.

Temperature (°C)	Stretching speed (mm/min)	Initial constant strain (%)	Preload (N)	Relaxation sampling time (s)
−40, −20, 0, 20, 40, 70	500	5	2	2, 4, 8, 20, 40, 80, 120, 200, 400, 600, 1000

Industry Standard of the Ministry of Aeronautics and Astronautics of the People's Republic of China QJ2487-93. Under the working conditions of solid engine transportation and storage, the temperature range it is subjected to is about −40 to 70°C [25, 26]. Therefore, in case of any discrepancy, the experimental conditions can be considered accountable.where $E(t)$ is the stress relaxation modulus at moment (t) (MPa), $F(t)$ is the relaxation force at moment $t\,(N)$, ε_0 is the initial constant strain (%), and A_0 is the specimen initial cross-sectional area (mm^2).

After the experiment is carried out according to Table 1 and calculations are performed using equation (1), the results are obtained and represented in Table 2.

$$E(t) = \frac{F(t)\left(1+\varepsilon_0\right)}{A_0\varepsilon_0}, \tag{1}$$

The changes in the structural relaxation of viscoelastic materials are dependent on the variations in production temperature and the life of their structures. If the change in temperature is extremely significant, it tends to alter the mechanical properties of the material. To ensure that the testing time does not become significantly long or short with temperature, it is necessary to obtain the logarithm of the temperature offset coefficient. Meanwhile, T_s is the reference temperature taken as 20°C, and isotherm curve of $\log(E(t)T_s/T)$ vs. $\log a_T$ corresponding to each test temperature T is shown in Figure 3. Translate each isothermal curve along the abscissa to 20°C of isothermal abscissa displacement value which is $\log a_T$. The specific method used can be found in the abovementioned standard [27]. In this way, the time-domain range of the equivalent relaxation modulus can be far more than 2–1800 s.

2.3. Fitting of Constitutive Equation. After fitting the above isothermal curve family, the relaxation modulus curve is obtained by using the temperature offset.

Table 2: Relaxation modulus at various temperatures.

T (°C)/t (s)	−40	−20	0	20	40	70
2	16.01	7.50	5.67	4.12	3.94	3.30
5	13.51	6.38	4.87	3.63	3.49	2.92
8	12.39	5.88	4.51	3.41	3.28	2.74
10	11.89	5.65	4.34	3.31	3.19	2.66
15	11.03	5.26	4.06	3.13	3.02	2.52
25	10.03	4.81	3.73	2.92	2.82	2.35
50	8.82	4.26	3.33	2.66	2.58	2.14
80	8.09	3.92	3.08	2.49	2.42	2.01
100	7.76	3.77	2.97	2.42	2.35	1.95
200	6.83	3.34	2.65	2.20	2.15	1.78
250	6.55	3.21	2.55	2.13	2.08	1.73
500	5.76	2.84	2.28	1.94	1.90	1.57
800	5.28	2.61	2.11	1.82	1.79	1.48
1000	5.07	2.51	2.03	1.77	1.73	1.43
1500	4.70	2.34	1.90	1.67	1.64	1.36
1800	4.55	2.27	1.84	1.63	1.61	1.33

The formula [28–33] used for Prony series fitting (as shown in Figure 4) of the relaxation modulus is as follows:

$$E(t) = E_0 + \sum E_i \exp\left(\frac{-X}{t_i}\right), \quad (i = 1 \sim 9), \tag{2}$$

where E_i is the transient modulus of the material and t_i is the Prony lag time constant. All the 19 parameters are shown in Table 3.

In this way, the constitutive equation of this viscoelastic material is developed.

3. Sinusoidal Frequency Sweep

The sinusoidal vibration test is divided into fixed frequency test and sweep frequency test, and the sweep frequency test is divided into linear and logarithmic frequency sweep modes. During the test, the frequency is always constant, that is, the constant frequency test.

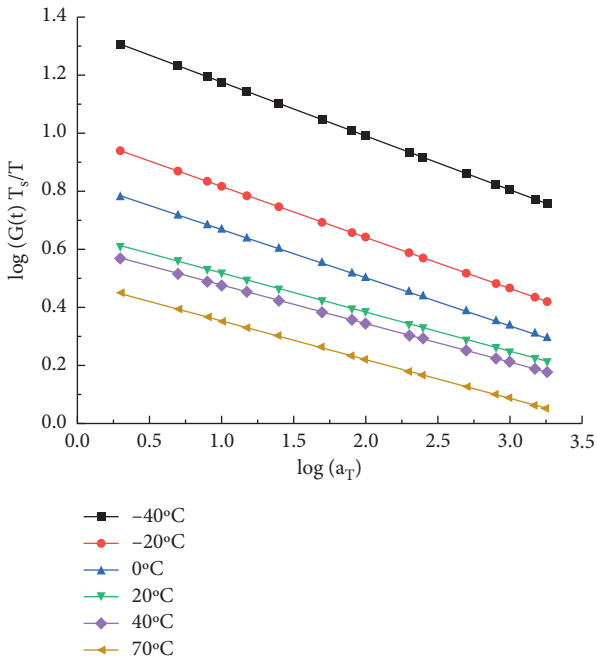

Figure 3: Isotherm family diagram.

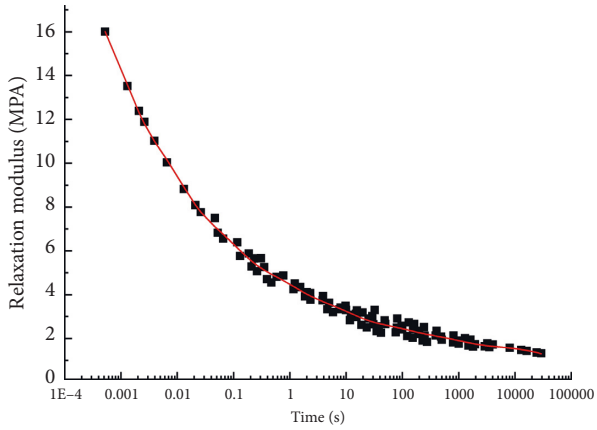

Figure 4: Master curve of relaxation modulus based on Prony series.

During the test, the frequency that changes with time is the frequency sweep test, and the vibration level in the frequency sweep test is a function of the frequency. The frequency sweep test is divided into linear frequency sweep and logarithmic frequency sweep according to the type of frequency change. Linear sweep frequency change is linear; log sweep frequency change is logarithmic.

3.1. Sinusoidal Frequency Sweep Set-Up. The sinusoidal sweep vibration test excites the test piece by continuously changing the vibration frequency in a certain frequency range, according to the prescribed vibration magnitude. The rate of change of the vibration frequency is called the scanning rate.

The relationship between the excitation frequency (f), testing time (t), and scanning rate (β) is expressed in the linear frequency sweep as follows:

$$\frac{df}{dt} = \beta(\text{constant}). \tag{3}$$

In logarithmic sweep, it is expressed as follows:

$$\frac{d(\text{inf})}{dt} = \beta(\text{constant}). \tag{4}$$

The starting frequency of the vibration test is recorded as f_0, and the starting time is recorded as t_0. Using equation (4), the relationship between the real-time frequency and t of the logarithmic sweep test is

$$f = f_0 \times e^{\beta(t-t_0)}. \tag{5}$$

A relatively simple functional relationship is observed between f and t during the linear frequency sweep test and the logarithmic frequency sweep test. Herein, the frequency scanning mechanism in sinusoidal frequency sweep test is known, and the starting time t_0 is defined by the data collector. Furthermore, the excitation frequency at any time can be calculated according to the frequency scanning mechanism by using t_0 only.

The yellow bench on the left is a self-made test bench (as shown in Figure 5), which is rigidly connected to the ground with bolts. A vibration exciter is placed on the test bench. The SIEMENS TESTLAB host is on the left, behind the exciter; a domestic amplifier is observed on the right, which controls the amplitude of signal amplification.

The figure on the right shows the clamping state of the viscoelastic cantilever beam. The size of the cantilever beam is 150 mm ∗ 40 mm ∗ 1 mm. For the sinusoidal vibration test, in view of the large operation error caused by the cutting of the specimen and the position of the sensor, only one specimen was made. From left to right, five sensors from the PCB Company are observed, of which No. 1, 2, 3, and 4 are accelerometers and No. 5 functions as a force sensor as well as an accelerometer (distributed upper and lower). The force sensor model is PCB-208C01, and the measurement range is 0 to 0.4448 KN. The accelerometer model is PCB-356A15, and the measurement range is 0 to 490 m/s^2. The force sensor is located at the source of the exciting vibration; therefore, the data it records can be considered a standard of the input exciting force. The clamping device is rigidly connected to the viscoelastic cantilever beam specimen, the test bench, and the ground.

3.2. Analysis of Experimental Modal. Select the 6 S-point marks that are relatively stable in the steady-state diagram, where the S-point mark indicates that the mode appears at this position, and then use the PloyMAX method to modal identification of the 6 S-points to obtain the corresponding sixth-order modal as shown in Figure 6.

After the test and calculation in SIEMENS TESTLAB itself, sixth-order modal frequencies are obtained [34–38] (Table 4).

Table 3: Parameters of Prony series fitting.

i	0	1	2	3	4	5	6	7	8	9
E_i (MPa)	0.301	6.512	4.291	2.572	1.455	1.203	0.550	0.604	0.054	1.348
t_i (s)		10–3	10–2	10–1	100	101	102	103	104	105

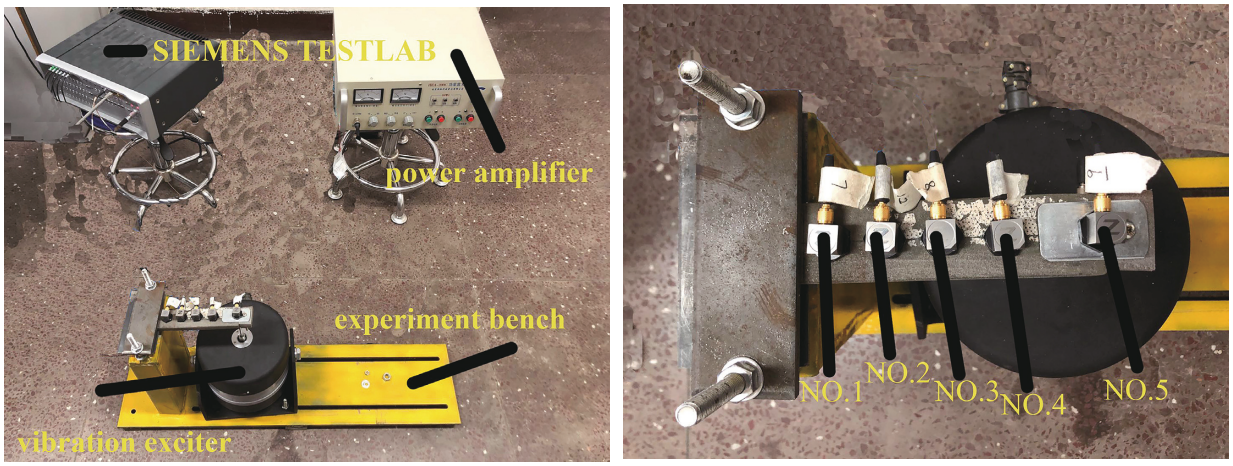

Figure 5: Vibration test bench.

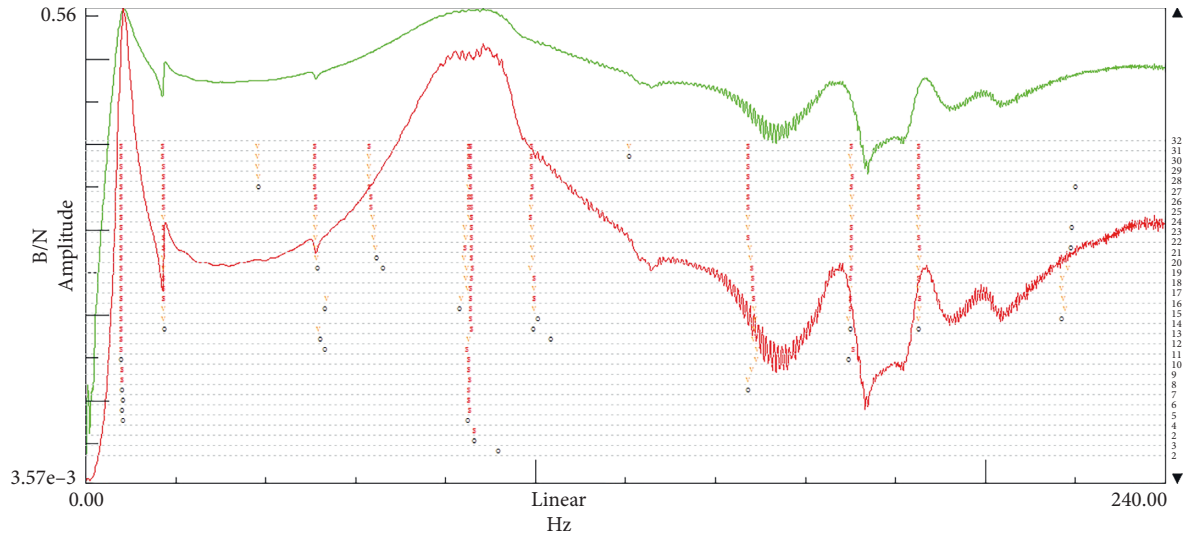

Figure 6: Steady-state graph based on Polymax.

Table 4: Sixth-order modal and frequency table.

Order	Frequency (Hz)	Damping ratio (%)	Participatory method
1	8.08	3.35	PolyMAX
2	17.30	3.75	PolyMAX
3	85.31	2.98	PolyMAX
4	148.04	4.22	PolyMAX
5	169.60	4.55	PolyMAX
6	238.06	3.97	PolyMAX

Although the continuum theoretically has an infinite number of natural frequencies, in many cases, we only care about low-order natural frequencies or specific-order natural frequencies. This is because the lower the natural frequency, the easier it is to be stimulated by the outside world. In addition, combined with the transportation and storage conditions of the propellant, the maximum frequency of the sinusoidal frequency sweep experiment is set at 80 Hz.

3.3. Sinusoidal Frequency Sweep Test. In the SIEMENS TESTLAB, the maximum frequency is set at 80 Hz, while the bandwidth, spectral line, resolution, capture time, and number of cycles are 80 Hz, 1024, 0.0781250 Hz, 10 s, and 30, respectively. Subsequently, the sinusoidal frequency sweep experiment is carried out. Since No. 5 acts as an

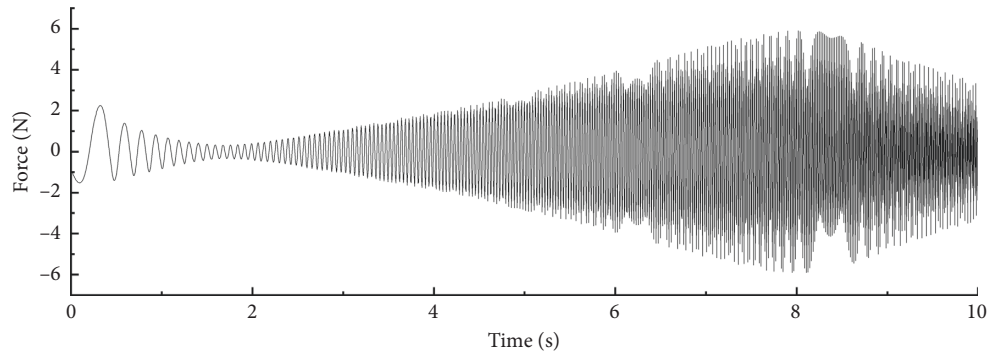

Figure 7: Measured input force values at point 5.

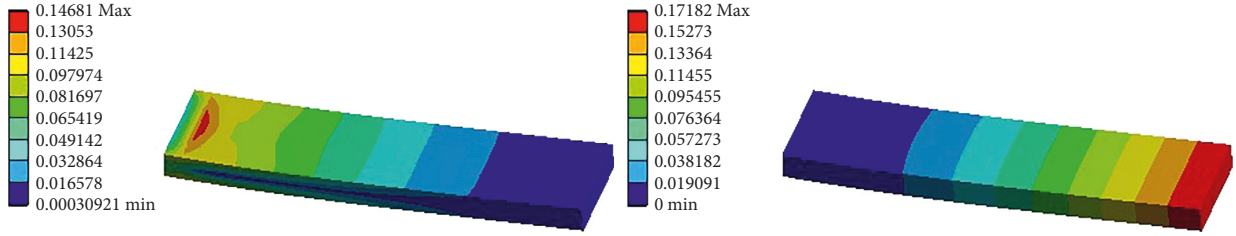

Figure 8: Strain and displacement contour.

accelerometer and a force sensor, the force data can be read in SIEMENS TESTLAB; these data are obtained after rectangular windowing and used as the reference input values for transient structure analysis. According to the results of the test measurement, the measured maximum force value is 5.90 N (as shown in Figure 7).

4. Finite Element Simulation and Analysis

The realization of finite element simulation is based on Workbench. Workbench is a collaborative simulation environment proposed by ANSYS to solve the heterogeneous problem of CAE software in the process of enterprise product development. The left end of the viscoelastic cantilever beam is constrained by a fixed end, which is realized with a self-made fixture. At the right edge is a concentrated load (infinitely close to the edge). The geometric model is realized by using the drawing function of the software [39, 40]. The length, width, and height of the cuboid model are 150, 40, and 10 mm, respectively. In the finite element simulation of viscoelastic materials, Prony series are mainly used to express its constitutive equation. The density of this material was measured to be 1700 kg/m^3, and Poisson's ratio was 0.495. All the elements are categorized according to their hexahedral solids. In the finite element method, the number of meshes is 64000 and the number of nodes is 281621. On this basis, the calculation shows good convergence. As observed, the maximum strain (as shown in the left in Figure 8) is 0.14681 and the maximum displacement (as shown in the left in Figure 8) is 0.17182 m.

The accelerations measured at the five points (by sensors No. 1 to No. 5) using the SIEMENS TESTLAB are exported and compared with those determined using finite element simulation. In the time domain, the simulated and measured accelerations at point 1 coincide well for the first 7 s; however, the overall simulated acceleration from 7–10 s is slightly smaller than the measured acceleration. The measured peak acceleration is 20.39 m/s^2, simulated peak acceleration is 20.88 m/s^2, peak acceleration error is 2.4%, and the simulated and measured peak accelerations appear at about 8 s. The simulated and measured accelerations at point 2 coincide well, and the peak acceleration also appears at approximately 8 s. The measured peak acceleration is 48.59 m/s^2, simulated peak acceleration is 49.70 m/s^2, and peak acceleration error is 2.28%. The simulated and measured values at point 3 do not coincide that well as those at point 2; however, both appear at 8 s. The measured peak acceleration is 59.50 m/s^2, simulated peak acceleration is 59 m/s^2, and peak acceleration error is 0.84%. At point 4, a good match is observed between the simulated and measured accelerations in the first 4 s, which becomes slightly worse from 4 to 8 s; however, the values still exhibit a reasonable match. The measured peak acceleration is 45.58 m/s^2, simulated peak acceleration is 45.53 m/s^2, peak acceleration appears at 8 s, and peak acceleration error is 0.10. At point 5, the measured peak acceleration is 41.82 m/s^2, simulated peak acceleration is 43.00 m/s^2, and peak acceleration error is 2.82%; the simulated peak acceleration appears at 9 s, which coincides with the time when the measured peak acceleration appears. Among the measured accelerations at the five points, the maximum acceleration of the cantilever beam appears at point 3 (59.50 m/s^2) and the minimum acceleration of the cantilever beam appears at point 1 (20.38 m/s^2). The maximum simulated acceleration of the cantilever beam appears at point 3 (59 m/s^2. The minimum acceleration appears at point 1 (20.88 m/s^2),

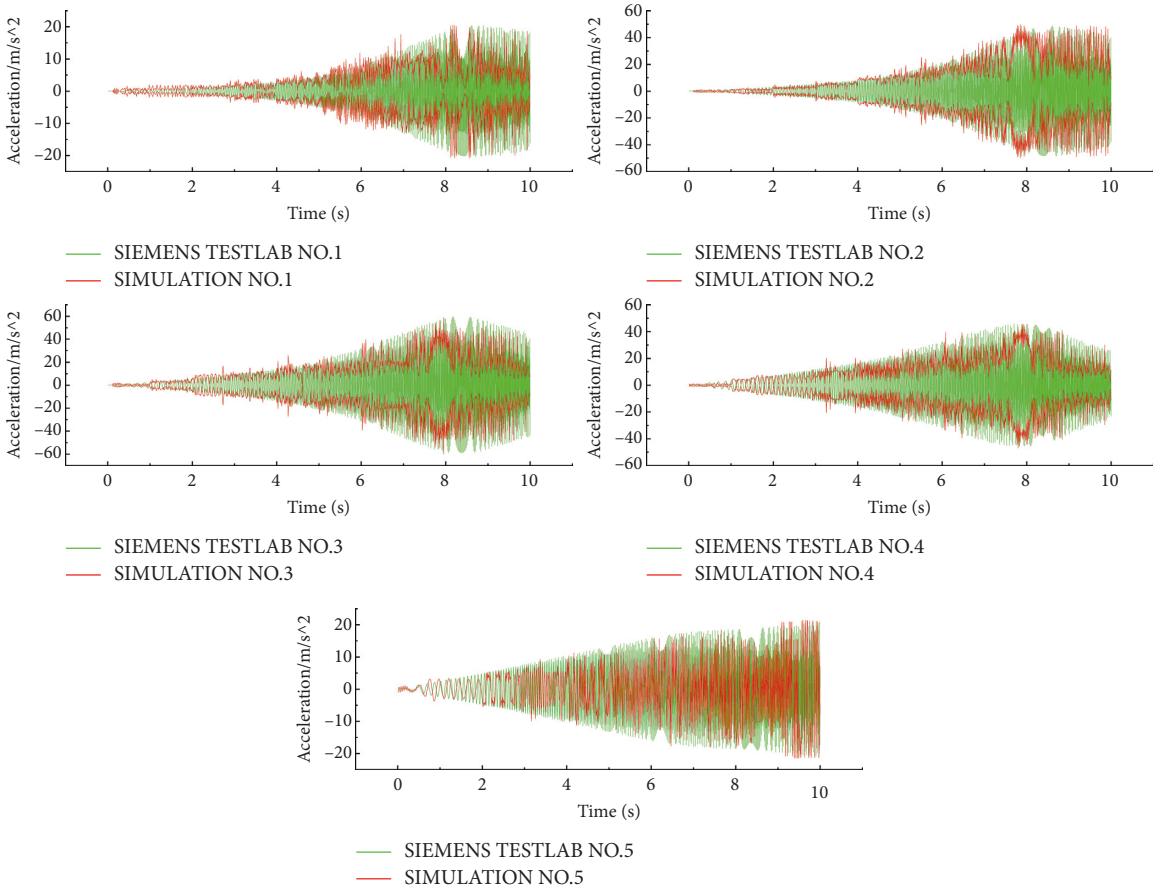

Figure 9: Measured and simulated accelerations at points 1 to 5.

Table 5: Maximum measured and simulated accelerations.

No.	Maximum measured acceleration (m/s^2)	Maximum simulated acceleration (m/s^2)	Relative error of simulation (%)
Point 1	20.39	20.88	2.40
Point 2	48.59	49.70	2.28
Point 3	59.50	59.00	0.84
Point 4	45.58	45.53	0.10
Point 5	41.82	43.00	2.82

and the simulated and measured values correspond well as shown in Figure 9 and Table 5.

In terms of the time domain, the peak errors of the simulated and measured values at the five points are all smaller than 3%. Furthermore, the peak accelerations also correspond well in the time domain.

5. Conclusion

This study carries out an experimental and simulation analysis on a viscoelastic cantilever beam, which analyzes the dynamic responses under dynamic conditions. The following conclusions are obtained:

(1) When the viscoelastic cantilever beam is sinusoidally excited, the maximum acceleration of the entire viscoelastic cantilever beam appears at the third point (the middle point), while the maximum acceleration of other linear materials appears at the fifth point (movable endpoint), and the two are the smallest. The accelerations all occur at point 1 (fixed endpoint), and the reason for this difference is that viscoelastic materials experience a combination of viscosity and elasticity when they are sinusoidally excited.

(2) In the sinusoidal excitation experiment, by measuring the acceleration response of the viscoelastic cantilever beam at points 1, 2, 3, 4 and 5, it is observed that the overall acceleration peak error and the finite element simulation result are less than 3%. The time-domain correspondence is satisfactory. The 19-parameter Prony constitutive equation can accurately describe the dynamic response of viscoelastic materials at low frequencies (<80 Hz). Therefore, the use of the 19-parameter Prony series

method to describe viscoelastic materials is still one of the most effective methods in simulation.

Future work will continue to study the dynamic response of viscoelastic material cantilever beams under random vibration.

Data Availability

The data supporting the conclusion of the article are shown in the relevant figures and tables in the article.

Conflicts of Interest

The authors declare that there are no conflicts of interest regarding the publication of this article.

Acknowledgments

This work was supported in part by the National Natural Science Foundation of China (11962021) and Inner Mongolia Natural Science Foundation Project (2021MS05020).

References

[1] L. Wei, *Identification of Fractional Derivative Viscoelasticity Model Parameters and its Finite Element Implementation*, Southwest Jiaotong University, Sichuan, China, 2018.

[2] H. Qian, Y. Wu, R. Zhu, and D. Zhang, "Modal Identification of Ultralow-Frequency Flexible Structures Based on Digital Image Correlation Method," *Applied sciences*, vol. 12, no. 1, 2021.

[3] J. Xu, Y. Ju, J. Zheng, and B. Han, "Acquisition of the relaxation modulus of composite solid propellant," *Chinese Journal of Explosives & Propellants*, vol. 34, no. 5, 2019.

[4] T. Miller, J. A. Louke, and C. S. Wojner, "Measuring propellant stress relaxation modulus using dynamic mechanical analyzer," *Journal of Propulsion & Power*, vol. 33, no. 5, 2017.

[5] Z. Zhou, X. Dong, Z. Li, K. Yu, C. Ding, and Y. Yang, "Spatio-temporal feature encoding for traffic accident detection in VANET environment," *IEEE Transactions on Intelligent Transportation Systems*, vol. 14, 2022.

[6] L. He, *Dynamic Analysis of Viscoelastic Materials Based on Prony Series and GHM Model*, Tsinghua University, Beijing, China, 2013.

[7] L. Zhao, H. Chai, Y. Han, K. Yu, and S. Mumtaz, "A collaborative V2X data correction method for road safety," *IEEE Transactions on Reliability*, vol. 55, pp. 1–12, 2022.

[8] G. M. Rowe, S. F. Brown, M. J. Sharrock, and M. G. Bouldin, "Viscoelastic analysis OF hot mix asphalt pavement structures," *J. Transportation Research Record*, vol. 12, 1995.

[9] H. Wang, *Design Optimization and Viscoelastic Response Analysis of Conductive Asphalt Pavement Based on Snow and Ice Melting*, Wuhan University of Technology, Hubei, China, 2010.

[10] D. Meng, Y. Xiao, Z. Guo et al., "A data-driven intelligent planning model for UAVs routing networks in mobile internet of things," *Computer Communications*, vol. 179, pp. 231–241, 2021.

[11] Y. Zhao, C. Zhou, G. Wang, and Z. Wang, "Analyses of viscoelastic responses of asphalt pavements under pulse loading," *Jersey Journal of Dalian University of Technology*, vol. 11, 2011.

[12] B. Wang and G. Zhang, "Analysis of dynamic response in three-dimensional viscoelastic large deformation," *J. Journal of Propulsion Technology*, vol. 20, 1994.

[13] X. Yuan and H. Sun, "Finite element analysis on viscoelastic properties of resin-based three-dimensional braided composites," *J. Chinese Journal of Applied Mechanics*, vol. 195, 2012.

[14] Z. Shi, C. Liu, and J. Yang, "Modified Riemann-Liouville fractional order derivative definition in solid propellant viscoelasticity constitutive model," *Chinese Journal of Applied Mechanics*, vol. 15, 2009.

[15] Z. Guo and H. Wang, "A deep graph neural network-based mechanism for social recommendations," *IEEE Transactions on Industrial Informatics*, vol. 17, no. 4, pp. 2776–2783, 2021.

[16] H. Zhou, L. Wang, H. Wang, and Y. Dai, "Viscous-elastic dynamic response for SRM grain under random loading," *Missiles and Space Vehicles*, vol. 20, 2019.

[17] J. Baqersad, P. Poozesh, C. Niezrecki, and B. Avaitabilie, "Comparison of Modal Parameters Extracted Using MIMO, SIMO, and Impact Hammer Tests on a Three-Bladed Wind Turbine," in *Proceedings of the Conference Proceedings of the Society for Experimental Mechanics Series book series (CPSEMS)*, Orlando, FL, USA, April 2014.

[18] W. Zheng and H. Chen, "Inverse multi-step prediction model method for MIMO random vibration test control," *Acta Aeronautica*, vol. 12, 2020.

[19] F. Zhu and Z. Deng, "Research on damage identification method based on random vibration response," *Annual Conference of Beijing Mechanics Society*, vol. 252, 2013.

[20] O. Yakaboski and A. V. Kumar, "Modeling and Simulation of RDX Powder Thermo-mechanical Response to Drop impact," *Propellants, Explosives, Pyrotechnics*, vol. 46, 2020.

[21] QJ 2487-1993, "Method for measuring uniaxial tensile stress relaxation modulus and master curve of composite solid propellant," 1993, https://www-bzgfw-com.translate.goog/forum.php?mod=misc&action=attachpay&aid=149529&tid=149521&_x_tr_sl=zh-CN&_x_tr_tl=en&_x_tr_hl=en&_x_tr_pto=sc&_x_tr_sch=http.

[22] J. J. Zhai, X. X. Kong, and L. C. Wang, "Thermo-Viscoelastic Response of 3D Braided Composites Based on a Novel FsMsFE Method," *Materials (Basel)*, vol. 14, 2021.

[23] R. W. Ogden, "Large deformation isotropic elasticity: on the correlation of theory and experiment for compressible rubberlike solids," *Proceedings of the Royal Society A: Mathematical*, vol. 326, 1972.

[24] P. H. Mott, C. M. Roland, and R. D. Corsaro, "Acoustic and dynamic mechanical properties of a polyurethane rubber," *Journal of the Acoustical Society of America*, vol. 111, 2002.

[25] Y. Wang, Y. Bai, X. Xu, J. Wang, and L. Li, "A Method for High-Accuracy Spectrum Analysis of Structural Response in Sine-Swept Vibration Test," *Journal of Spacecraft Environment Engineering*, vol. 983, 2020.

[26] H. Roy and S. Chandraker, "Dynamic study of viscoelastic rotor: modal analysis of higher order model considering various asymmetries," *Journal of Mechanism and Machine Theory*, vol. 109, 2017.

[27] N. Mills, "Finite element models for the viscoelasticity of open-cell polyurethane foam," *Journal of Cellular Polymers*, vol. 25, 2006.

[28] M. Liu, "Frequency Domain Method of the Crack Growth Life Analysis for Structure Vibration Fatigue," *Nanjing University of Aeronautics and Astronautics*, vol. 47, 2017.

[29] H. Fouad, A. Mourad, B. A. Alshammari, and M. K. Hassan, "Fracture toughness, vibration modal analysis and viscoelastic

behavior of Kevlar, glass, and carbon fiber/epoxy composites for dental-post applications," *Journal of the Mechanical Behavior of Biomedical Materials*, vol. 101, 2019.

[30] H. Shuai, C. Wen, and X. Gou, "Modal analysis of fractional derivative damping model of frequency-dependent viscoelastic soft matter," *Advances in Vibration Engineering*, vol. 10, no. 3, 2016.

[31] E. D. Lorenzo, S. Manzato, B. Peeters, and V. Ruffini, "Modal Analysis of Wind Turbine Blades with Different Test Setup Configurations," *Topics in Model Analysis and Testing*, vol. 8, 2020.

[32] W. Xie and Z. Zhang, "Dynamic Test and Analysis of the Structure of the Stadium Stand in Suzhou Industrial Park," *Applied sciences*, vol. 12, 2021.

[33] S. H. Wang, L. Zhang, and T. Li, "Vibration test analysis and control of solid rocket motor," *J. Computer Measurement and Control*, vol. 57-63, 2017.

[34] R. M. Hidalgo, J. G. Fernandez, R. R. Rivera, and H. A. Lorrondo, "A simple adjustable window algorithm to improve FFT measurements," *IEEE Transactions on Instrumentation and Measurement*, vol. 51, 2002.

[35] H. Zheng, J. P. Ertel, M. Kourmpetis, and J. Kanfoud, "Integrity testing of cast in situ concrete piles based on an impulse response function method using sine-sweep excitation by a shaker," *Journal of Non-destructive Evaluation*, vol. 55, 2019.

[36] Y. F. Wang, G. C. Li, and X. W. Wang, "Storage and life prediction of solid rocket motors in marine environment," *Chinese Journal of Explosives & Propellants*, vol. 66, 2008.

[37] Z. Li, *Viscoelastic Fractional Derivative Model and its Application to Solid Motors*, Tsinghua University, Beijing, China, 2000.

[38] A. Plouin and E. Balmès, "Steel/viscoelastic/steel sandwich shells," in *Proceedings of the Computational Methods and Experimental Validations//International Modal Analysis Conference*, Honolulu, Hawaii, December, 2000.

[39] G. Xia, T. Zhao, and L. Guan, "Enhanced thermal and mechanical properties of PW-based HTPB binder using polystyrene (PS) and PS–SiO_2 microencapsulated paraffin wax (MePW)," *Journal of Applied Polymer Science*, vol. 110, 2018.

[40] H. B. Li and Y. B. Li, "Experimental study on Poisson's ratio of viscoelastic grain," *The Journal of New Industrialization*, vol. 61, 2016.